Contents lists available at ScienceDirect

Journal of Power Sources

journal homepage: www.elsevier.com

Effect of overcharge on $Li(Ni_{0.5}Mn_{0.3}Co_{0.2})O_2$/Graphite lithium ion cells with poly(vinylidene fluoride) binder. I. Microstructural changes in the anode

Nancy Dietz Rago[a, *], Javier Bareño[a], Jianlin Li[b], Zhijia Du[b], David L. Wood III [b], Leigh Anna Steele[c], Joshua Lamb[c], Scott Spangler[c], Christopher Grosso[c], Kyle Fenton[c], Ira Bloom[a]

[a] Chemical Sciences and Engineering Division, Argonne National Laboratory, Argonne, IL 60439, USA
[b] Energy and Transportation Science Division, Oak Ridge National Laboratory, Oak Ridge, TN 37831, USA
[c] Power Sources Technology Group, Sandia National Laboratories, Albuquerque, NM 87185, USA

ARTICLE INFO

Keywords:
Lithium-ion battery
Overcharge
Scanning electron microscopy
Microstructure
SEI
Anode

ABSTRACT

Cells based on NMC/graphite, containing poly(vinylidene difluoride) (PVDF) binders in the positive and negative electrodes, were systematically overcharged to 100, 120, 140, 160, 180, and 250% state-of-charge (SOC). At 250% SOC the cell vented. Scanning electron microscopy (SEM) and energy dispersive spectroscopy (EDS) of the anodes showed several state-of-overcharge-dependent trends. Starting at 120% SOC, dendrites appeared and increased in concentration as the SOC increased. Dendrite morphology appeared to be dependent on whether the active material was on the "dull" or "shiny" side of the copper collector. Significantly more delamination of the active material from the collector was seen on the "shiny" side of the collector particularly at 180 and 250% SOC. Transition metals were detected at 120% SOC and increased in concentration as the SOC increased. There was considerable spatial heterogeneity in the microstructures across each laminate with several regions displaying complex layered structures.

1. Introduction

Lithium-ion batteries are an important energy source due to their high energy and power density, however, the demand for increased performance, particularly in electric vehicles (EVs), has highlighted safety concerns and limited battery lifetime. One way of increasing energy storage would be to add more strings of cells in parallel to the battery pack in EVs. But, with each additional string of cells, there is a performance penalty due to its weight. Another, perhaps better, solution would be to use higher-energy materials in the battery pack.

High-nickel-containing cathode materials, such as $Li(Ni_{0.5}Mn_{0.3}Co_{0.2})O_2$ (NMC532), have been proposed for this purpose. Cells containing NMC532 typically have higher capacity densities, and hence, higher energy densities, as compared to materials with lower nickel concentrations (175 vs. 160 $mA\,g^{-1}$ for NMC(1:1:1)) [1].

With increased energy content of the cathode material, there may be additional safety concerns in cells containing these materials. Among these safety issues, overcharge (OC) is one of the most common and hazardous problems associated with commercial Li-ion batteries. Overcharge occurs when a charging current is forced through the battery after it has reached its end-of-charge potential, raising the cell potential to higher values [2]. At certain high potentials, de-lithiation at the cathode and a corresponding excess of lithium at the anode can result in the formation of dendrites that can puncture the separator and short circuit the cell. Short circuits can generate high current, leading to a rapid increase in temperature. Finally, sustained overcharge will generate high internal temperature increases beyond the manufacturer's specifications. Combined with high pressure increase, this condition will lead to thermal runaway and ultimately to catastrophic rupture [3].

Because of the serious hazardous consequences of overcharge, particularly in modular systems where failure can propagate from cell to cell, understanding the physical and chemical changes of overcharging the cell is extremely important for the development of safe batteries that can be used in an EV. With this information, the abuse response may be mitigated by appropriate changes in the cell chemistry, such as selecting appropriate additives [4–6] that coat the cathode or are added to the electrolyte. However, there is very little systematic infor-

* Corresponding author.
Email address: dietz@anl.gov (N. Dietz Rago)

https://doi.org/10.1016/j.jpowsour.2018.01.009
Received 18 September 2017; Received in revised form 5 December 2017; Accepted 4 January 2018
Available online xxx
0378-7753/

mation in the literature describing what happens during each stage of the overcharge event.

Yuan et al. [7] overcharged 32-Ah cells containing NMC(1:1:1) cathodes at the 1-C rate. The cells were overcharged in steps: 100%, 170%, 180%, 190% and 200 + % SOC. They observed that the skin temperature of the cell increased rapidly at about 200% state-of-charge before going into thermal runaway. Analysis of the gases in the cell showed that CO_2 increased with SOC in the range of 100%–190% SOC. Post-test analysis showed that lithium plating on the anode was the primary cause of cell failure.

Makimura et al. [8] investigated the overcharge behavior of cells containing $LiNi_{0.75}Co_{0.15}Al_{0.05}Mg_{0.05}O_2$ cathodes. They overcharged the cells at 30 °C and 50 °C towards 10 V. Their X-ray absorption near edge structure (XANES) results showed that the entire spectrum of the cathode monotonously shifted to higher energy with overcharge. They interpret these observations as indicating that the Ni in their material was being oxidized. Their X-ray diffraction results indicate that the graphite anode transforms to LiC_6 until it cannot contain additional lithium, after which the "lithium flows over from the graphite," suggesting lithium plating [9]. Indeed, examination of the anode after the experiment showed that lithium plating was present.

The impact of overcharge has been explored using $LiFePO_4/Li_4Ti_5O_{12}$ [9], $LiCoO_2$/graphite [10,11] and $LiFePO_4$/graphite [10,12–14] cells from the fundamental viewpoint, such as how just the graphite anode material changes during an overcharge event [15,16], using post-test disassembly as well as in-situ methods. On the other hand, there is a report of techniques to determine the effect of overcharging an NMC (1:1:1)/$Li_4Ti_5O_{12}$ cells without the need for post-test disassembly [17].

In the present study, Argonne National Laboratory (Argonne), Oak Ridge National Laboratory (ORNL), and Sandia National Laboratories (SNL) collaborated to better understand the physical and chemical changes associated with the stepwise overcharge of NMC532/graphite cells made with *N*-methylpyrrolidinone (NMP)-soluble binders. Here, the cells were charged to 100, 120, 140, 160, 180, and 250% SOC (0, 20, 40, 60, 80, and 150% overcharge). After overcharge, the cells were discharged to 0% SOC and subsequently disassembled in an argon-filled glovebox.

This paper represents the first in a series of three papers that each focus on:

I) microstructural changes in the anode that were observed by scanning electron microscopy (SEM) with energy dispersive spectroscopy (EDS);
II) chemical changes in the anodes measured by inductively-coupled-plasma mass spectrometry (ICP-MS), X-ray photoelectron spectroscopy (XPS), and high-performance liquid chromatography (HPLC) [18]; and
III) changes in the cathode measured by XPS, X-ray diffraction (XRD), and solid-state nuclear magnetic resonance (SSNMR) [19].

2. Experimental

2.1. Materials

1.5-Ah pouch cells were fabricated at ORNL. They consisted of $Li(Ni_{0.5}Mn_{0.3}Co_{0.2})O_2$ cathodes (NMC532, Toda America), Celgard 2325 separators, and graphite (A12, ConocoPhillips) anodes. Here, the double-side cathode laminate consisted of 90 wt% NMC532, 5 wt% Denka carbon black (powder grade) and 5 wt% polyvinylidene fluoride (Solvay Solef® PVDF 5130) binder. The loading density of the cathode was 12.5 mg cm^{-2}. The cathode material was spread on 15 μm-thick aluminum foil (MTI Corporation) and was 50 μm thick on each side after calendaring, corresponding to 40% porosity.

Similarly, the anode laminate consisted of 92 wt% A12 graphite, 2 wt% carbon black (C-NERGY Super C65, Imerys Graphite & Carbon), and 6 wt% PVDF (PVDF, Kureha 9300) binder. The loading density of the anode was 6.5 mg cm^{-2}. The slurry preparation and electrode coating have been reported previously [20]. The anode material was spread on 9 μm-thick copper foil (MTI Corporation) and was 48 μm thick on each side after calendaring, corresponding to 37% porosity.

Based on the specific capacity of 330 mAh/g for graphite and 165 mAh/g for NMC, the areal capacities were 1.86 and 1.97 mAh/cm2 for the cathode and anode, respectively, with an N/P ratio of 1.06. In this study, the copper foil current collector had a "dull" side with exposed Cu grain boundaries, and a "smooth" side with the typical microstructure of rolled copper [S1].

The electrolyte consisted of 1.2 M $LiPF_6$ in ethylene carbonate:diethylcarbonate (3:7 by wt.). The cells were formed by charging/discharging at the C/20 rate between 2.5 and 4.2 V for 4 cycles.

After formation, the cells were shipped to SNL. The cells were then instrumented with thermocouples, voltage sense leads, and current-carrying cables; and fixed in phenolic constraints. A Bitrode battery tester was used to carry out the overcharging as well as to discharge them after the overcharge test. A constant current charge rate of 1C (1.5 A) was applied to the cells to reach the desired state of overcharge. Cells were set to 100% (no overcharge), 120%, 140%, 160%, 180%, and 250% SOC (failure, compliance voltage of 20 V met). The overcharge was followed by a 30-min rest and a discharge at the 1-C rate to 2.5 V. If the cell exceeded a voltage of 2.8 V after a 30-min rest, then a subsequent discharge was performed. Depending on the level of overcharge, multiple discharges were performed in an attempt to remove capacity and reduce voltage to satisfy shipping requirements. The higher states of overcharge exhibited increased impedance so large polarization was seen with attempts to decrease the cell voltage for shipment. Once the 2.8 V was met, the cell was monitored to understand the voltage recovery. The cells were shipped to Argonne in this state for post-test analysis.

3. Post-test characterization

In an argon-filled glovebox, the cells were opened using ceramic scissors. The electrodes were removed from the separator ribbon and allowed to dry. Sections of the separator and positive and negative electrodes were cleaned two times by swirling one minute each in excess dimethylcarbonate.

Sections were placed in an airtight holder, which was based on the design published by ORNL [21]. After mounting the sample, the sealed assembly was removed from the glove box and evacuated. After evacuation, the lid screws were removed and the holder was placed in a JEOL JSM-6610LV scanning electron microscope. In the SEM column, the holder lid opened when the vacuum in the column exceeded the vacuum inside the holder. Energy-dispersive spectroscopy (EDS) was performed using an Oxford Instruments XMax^N detector (detector size = 50 mm^2) and AZtecEnergy® software.

4. Results and discussion

The relationship between cell voltage and an increasing SOC is shown in Fig. S2 (see Appendix). Cell voltage increased linearly with SOC until 250% SOC. At that point, the cell voltage increased to that of the power supply. All cells, except that charged to 250% SOC, survived overcharging. The cell charged to 250% SOC vented. Fig. S3 (see Appendix) shows the external cell temperature as a function of SOC. The temperature increased linearly with increasing SOC.

4.1. Initial disassembly

No obvious signs of physical damage were seen in the electrodes from the 100%–140% SOC cells. Starting with the 160% cell, some of the anode material was stuck to the separator. Changes in the anode surface are shown in Fig. 1. Notice that variation in surface features was seen among anodes within a cell. This is most noticeable with an increasing SOC, particularly evident in the 160% through 250% SOC cells.

Direct visualization upon disassembly provided the first observation indicating degradation during overcharge was associated with local inhomogeneities across the laminate surface. As the images taken during disassembly show, there was considerable surface discoloration along with varying degrees of delamination of the active layer from the collector. Even after rinsing in dimethyl carbonate (DMC), presumably removing precipitated salts and soluble reaction products, the majority of discoloration on the anode surface remained.

This variation across the laminate could represent areas that have become electrically disconnected from the current collector, regions of varying current density distribution, variation in concentration of electrolyte salt, and non-uniform distribution of reaction products. Disassembly showed increasing delamination of the active material from the collector, particularly in the 180% and 250% SOC cells. Visual color variation associated with dendrites became evident in the 140% SOC cell where these areas appeared to have a grayish-beige or "ashy" color.

4.2. Microscopy

SEM examination showed the anode microstructure of the 100% and 120% SOC cells did not appear to be altered from the pristine anode microstructure. There was no discernible appearance of an SEI layer or microstructures indicating Li deposition. EDS analysis showed trace Ni on the 120% SOC anode, indicating some dissolution of the cathode active material and subsequent migration of cathode transition metals to the anode surface. As Ni is present in the highest concentration, Mn and Co were probably too low to detect.

Fig. 2 shows representative images of 100% and 120% SOC anode surfaces.

Dendrites started to appear at 140% SOC, with the dendrite concentration increasing with an increasing SOC. It should be noted that, starting with 140% SOC, adherence of some electrode material to the separator was noticed in the cells. Throughout the anode surface, there were varying degrees of anode pull away. Consequently, the microstructural representations of the surface had to be constructed by observing several areas on the anode and on the corresponding separator.

EDS analysis detected some Ni, Mn, and Co on the surface of the anodes, starting at 120% SOC. These concentrations tended to increase with increasing overcharge.

At 140% SOC, the anode surfaces were partially covered with dendrites that incorporated the transition metals. Presumably, these "islands" of dendrites were what remained after pulling the separator away during disassembly. Examination of the separator confirmed the attachment of dendrite aggregates on the surface. Fig. 3A is a backscattered electron image, which provided atomic number contrast. The image shows distinct graphite particles (on the left) and graphite covered with dendrites (on the right). The backscattered electron contrast shows that the transition metals were found primarily in the dendrites. Fig. 3B shows a dendrite surface aggregate on top of graphite particles.

The presence of dendrites at 140% SOC implies that extracted Li from the cathode is now depositing on the anode surface faster than the kinetics of graphite intercalation. The subsequent plating of Li results in the formation of dendrites covering most of the laminate surface.

The dendrites appeared to be either smooth or coated. Fig. 4 shows both smooth and coated dendrite morphology. The coating had nanoscale particles embedded in it that contained transition metals.

Why there were coated and uncoated dendrites may be related to differences in current density. It is well known that Li morphology changes with current density. Orsini showed that mossy Li was formed at low current density, while dendrites were formed at high current density [22]. Higher temperatures favored a more nodular structure over dendritic and also increased transport through the SEI layer [23]. In general, the shiny side appeared to have more coated dendrites than

Fig. 1. Images of anodes taken after disassembly in the glovebox. Anode surfaces exhibit changing surface features with an increasing SOC. From 160% to 250% SOC, delamination from the collector is evident.

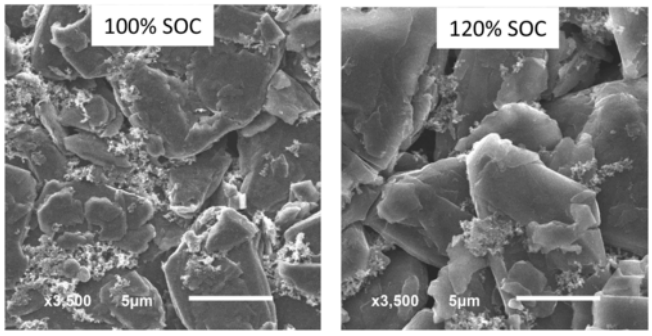

Fig. 2. Representative anode surface microstructure at 100% and 120% SOC.

the dull side, but this observation might be an artifact from disassembly, i.e., there was more pull out of anode material due to adherence to the separator. Extensive surveillance of the anode surface showed that, in some areas, the coated dendrites coexisted with smooth dendrites. Here, the coated dendrites appeared to be more superficial while the smooth dendrites appeared to be only in intimate contact with the graphite particles.

Zhang et al. [23] described a scenario for dendrite growth that could explain this observation. As Li dendrites grow from the graphite surface, they are covered by a thin SEI layer [23,24]. During dissolution, the remaining Li was no longer continuous and it became trapped within the SEI, creating electrochemically inactive Li, with just the SEI in contact with the graphite. When deposition occurs again, the top layer is pushed outward by the new dendrites growing on the exposed graphite. The inactive Li may mask some of the graphite, reducing the active surface area that is available for deposition, and increasing the effective current density. With increasing current density, rising temperature associated with overcharge, and changes in the SEI composition as a result of degradation reactions, the dendrite becomes increasingly coated with electrolyte decomposition products and transition metal particles. This would explain why the superficial dendrites were coated while the deeper newer dendrites in contact with the graphite were uncoated and appeared to be smooth.

Some of the smooth dendrites that were seen only on the exposed graphite particles (due to pull out of the anode onto the separator during disassembly) appeared to be hollow. Fig. 5A shows cross sections of dendrites (red arrow) growing through the cracked SEI layer. Fig. 5B is

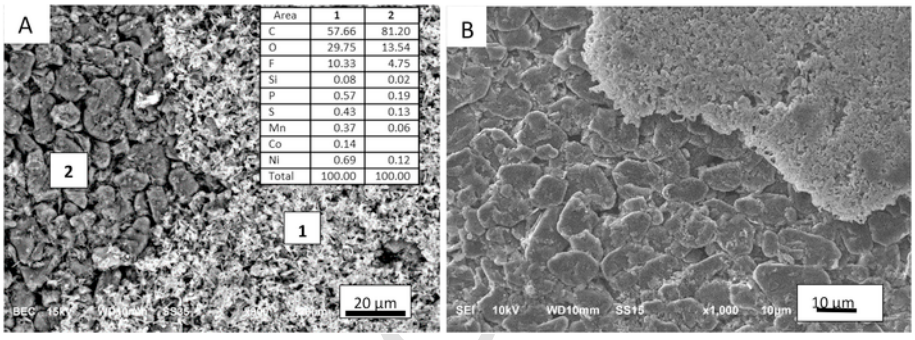

Area	1	2
C	57.66	81.20
O	29.75	13.54
F	10.33	4.75
Si	0.08	0.02
P	0.57	0.19
S	0.43	0.13
Mn	0.37	0.06
Co	0.14	
Ni	0.69	0.12
Total	100.00	100.00

Fig. 3. 140% SOC. A) Backscattered electron image of anode surface showing distribution of transition metals mainly associated with dendrites. B) Dendrite surface aggregate on top of graphite.

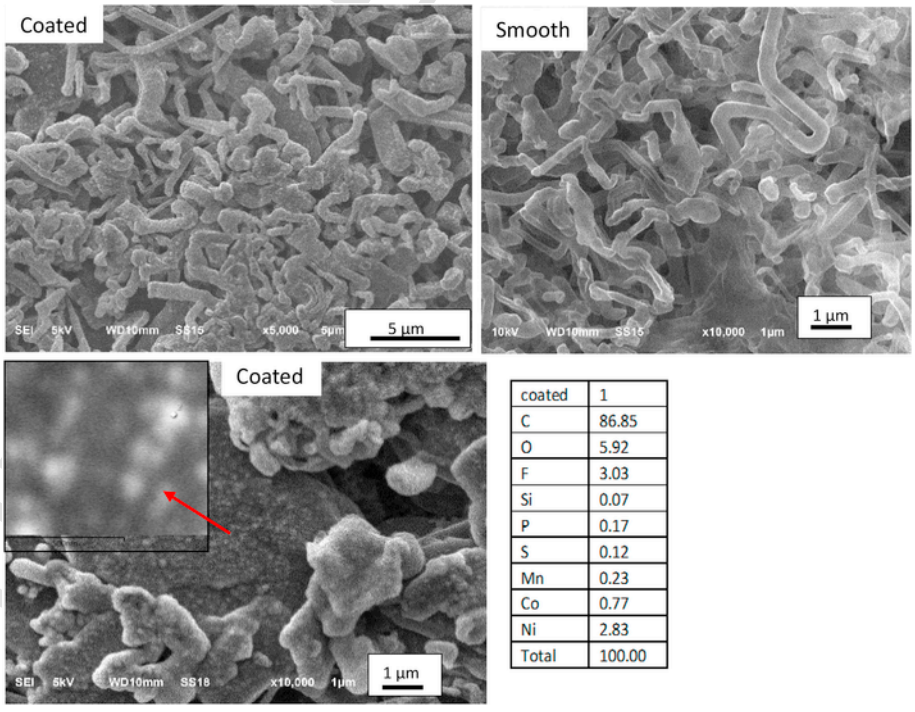

coated	1
C	86.85
O	5.92
F	3.03
Si	0.07
P	0.17
S	0.12
Mn	0.23
Co	0.77
Ni	2.83
Total	100.00

Fig. 4. 140% SOC. Smooth and coated dendrites on 140% SOC anode surface. EDS analysis shows that small particles on the dendrites and graphite particles are associated with transition metals.

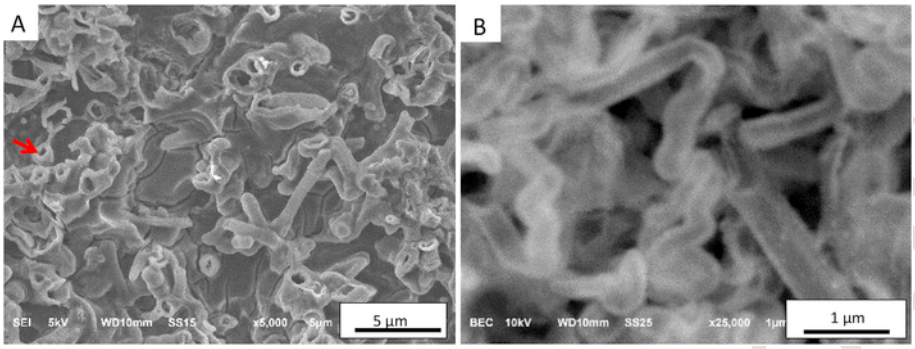

Fig. 5. A) 250% SOC. Dendrites associated with SEI layer. Several are seen in cross sections (red arrow). B) 140% SOC. Backscattered electron image showing higher atomic number contrast surrounding dendrites. (For interpretation of the references to color in this figure legend, the reader is referred to the Web version of this article.)

a backscattered electron image showing higher atomic number contrast material surrounding dendrites.

Theories of dendrite growth describe the dendrite as a metallic outgrowth surrounded by a thin SEI layer [23–25]. In our study, transition metal reaction products were precipitated on top of the SEI layer. The dendrites that appear hollow in Fig. 5A are in intimate contact with graphite and may have lost their internal lithium during a discharge subcycle, making them appear hollow.

At 160% SOC, there was a dense, homogeneous dendrite coverage across the laminate along with areas of layered surface structures. There were visible differences between the anode surfaces on the dull and shiny sides of the collector. The anode had an ashy-colored side associated with the dull side of the collector, and a darker grey-colored side associated with the shiny side of the collector. The dull ashy side appeared homogeneously covered with dendrites, whereas the shiny side appeared to have undergone extensive pull out, as evidenced by patches of dendrites on the corresponding separator surface. Most of the dendrites on the shiny side appeared heavily coated. Fig. 6 shows the dendrite distribution and morphology of the dull and shiny sides of the electrode. Transition metals, associated with the dendrites, are now present in higher concentration than in the 140% SOC.

EDS analysis of these coated dendrites showed higher concentrations of transition metals than those detected at the lower states of charge, indicating increased metal dissolution from the cathode and presumably more side reactions at high SOCs.

The shiny side anode now has a more nodular morphology consisting of round particles, ~300 nm in diameter, clumped together. This is most likely another morphology of Li deposition, which can be nodules that are fused together [23]. The emergence of the nodular morphology is an indication that temperature, current density, and electrolyte composition are changing with increasing SOC. In some regions, these nodular structures are comingled or covered with a smooth amorphous

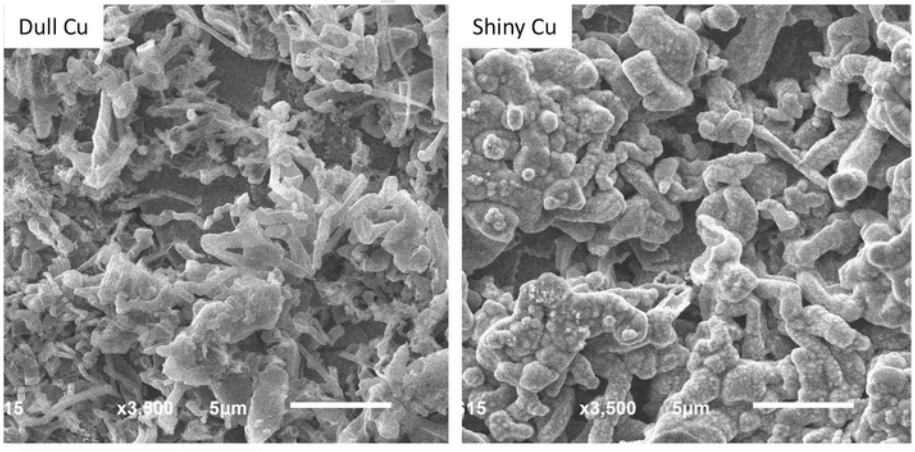

Area	1	2
C	36.45	29.65
O	24.82	21.91
F	22.77	32.25
Si		0.11
P	1.40	1.94
S	0.27	0.48
Mn	1.69	2.83
Co	3.63	3.03
Ni	8.51	7.39
Cu	0.47	0.42
Total	100.00	100.00

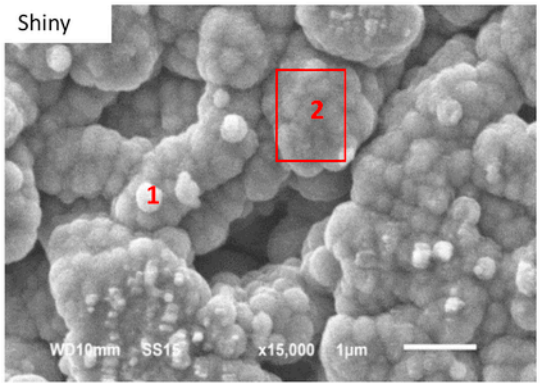

Fig. 6. 160% SOC anode dendrites on the dull and shiny sides of the collector. The EDS table shows the presence of transition metals on the dendrite coating.

appearing material that is also present, to a greater extent, on the corresponding separator surface. This material is also seen in the remaining cells (180% and 250% SOC).

Delamination of the active material from the collector is evident starting at 160% SOC. As the SOC increases, irreversible structural changes and decomposition of active material occurs at the cathode for many cathode chemistries [26,27]. These reactions generate a large amount of oxygen and heat. If at 160% SOC enough oxygen is generated, oxidation of the collector will enhance delamination.

By 180% SOC, dramatic changes have occurred in the microstructure. This is an indication that reactions between the cathode and electrolyte are occurring faster and are more exothermic. In an overcharge study conducted by Yuan et al. [28] on cells consisting of $Ni_{0.33}Co_{0.33}Mn_{0.33}O_2$ as the cathode and carbonaceous microspheres as the anode, ICP analysis was used to measure the relationship between Li content and SOC. Their results show a nearly linear increase in Li with increasing SOC until 180% SOC. After 180% SOC, very little Li is detected. They surmise that after 180% SOC it is difficult to remove the remaining Li in the cathode, consequently electrolyte decomposition and side reactions dominantly affect capacity. These results represent a turning point in overcharge reaction trends that could be manifested by the type of microstructural changes seen here at 180% SOC.

New surface species in addition to the sequence of reactions now further complicate the surface film morphology, resulting in multilayer structures [29,30] and a corresponding nonuniform current distribution associated with Li deposition/dissolution [30]. Evidence of the increasingly complex chemistry on the anode surface was the existence of three distinct layers over the graphite as shown in Fig. 7. Transition metal distribution was highest in the most superficial layer (layer 1) and in the dendrite layer (layer 3). Layer 1 could represent another morphology of Li deposition. The SEI layer, in between, had trace concentrations of transition metals, most likely contributions from the top and bottom layers. In spite of pull out onto the separator during disassembly, these five layers are probably not homogeneously developed throughout the anode surface. Areas with fewer layers or even different microstructures could evolve due to local fluctuations in current density, amount of electrolyte, and delamination from the collector.

In a previous study [31], the morphological characterization of the SEI layer formed in a cell containing $LiClO_4$ EC/PC showed SEM images of an SEI structure that looks the same as the amorphous material seen here (layer 2). If this material, indeed, represents remnants of an SEI layer, then it can be said that the SEI is not uniform across the laminate surface. The cracking might provide the first evidence of SEI breakdown during overcharge or could be caused by drying of laminate during handling. EDS analysis consistently detected relatively high levels of F and P in this material. Bearing in mind that EDS does not detect Li, and assuming that Li is present, P and F are major components of the SEI [32,33]. Several studies report LiF, a major salt reduction product, and Li_2CO_3, a precipitate from Li-ions and electrolyte solvent carbonates, as the main constituents of the SEI in systems that contain $LiPF_6$ salts [32,34,35]. XPS [18] suggests that the concentration of Li_xPOF_y in the SEI layer increases with higher states of charge. These results support the microscopy and EDS data that show increasing F and P associated with more complicated and thicker surface structures.

At 250% SOC, the cell vented as the external temperature reached 100 °C. The microstructure is dominated by heavily coated dendrites, but there is significant pull out of the anode onto the separator along with delamination of the active layer from the collector, making microstructural spatial relationships extremely difficult to establish. Fig. 8 shows the dense concentration of matted dendrites on the anode surface.

Extensive delamination of the active layer from the collector along with the final event of venting is possible evidence that moisture and oxygen released from electrolyte decomposition and structural deformation of the cathode has increased [28]. Fig. 9 shows anode material that adhered to the separator upon disassembly.

Because of the extensive pull out of the anode surface onto the separator, an effort was made to obtain a more intact anode surface that would be representative of the microstructure. A piece of anode that was stuck to the separator was soaked in dimethylcarbonate for ~2 h, then gently pulled apart. In comparison to the standard protocol of rinsing pieces two times for ~1 min each, the extended soaking produced less pull out of the anode surface material onto the separator.

Both sides (dull and shiny) showed localized areas of a polymeric substance that could be redistributed binder. It did not have the characteristic surface porosity of the separator and contains F, although F could be present everywhere at this SOC. Fig. 10 shows the anode surface after soaking in DMC for two hours. In Fig. 10A the surface has strands of polymeric material that appears pulled out during the separation of the anode from the separator. A higher magnification of this

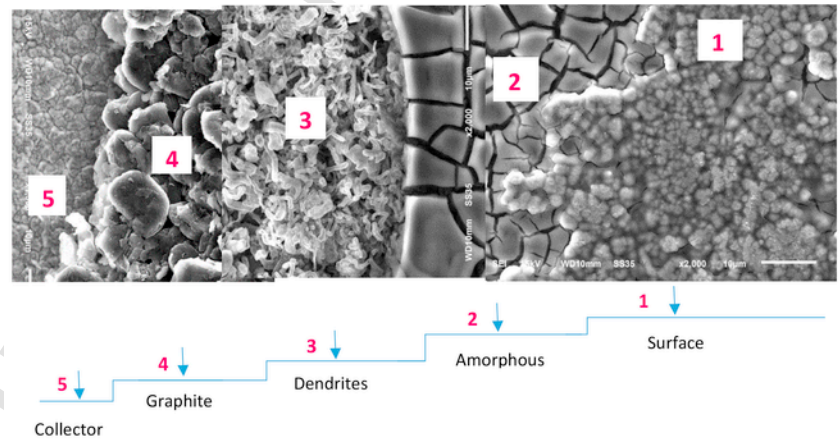

Area	C	O	F	P	S	Mn	Co	Ni	Cu
1	42.25	32.48	11.45	2.06	0.13	0.96	3.76	6.69	
2	23.63	14.44	54.37	6.06	0.33	0.37	0.25	0.70	
3	45.09	32.48	9.50	1.65	0.17	1.20	3.33	6.28	
4	89.41	5.57	4.75	4.75					0.05

Fig. 7. 180% SOC. Anode surface layers and corresponding EDS data.

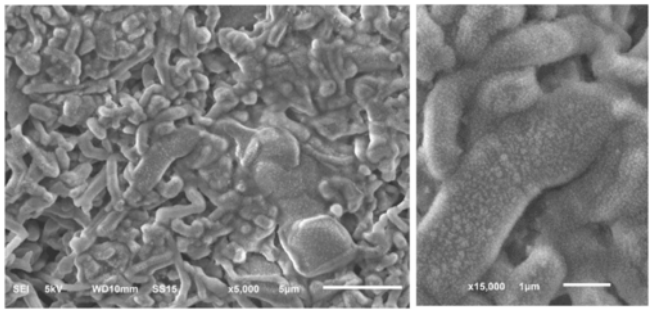

Fig. 8. 250% SOC. Heavily coated densely packed dendrites dominate the surface.

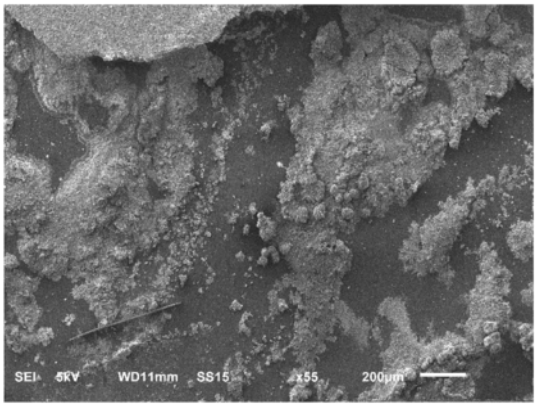

Fig. 9. 250% SOC. Surface of the separator in contact with the anode showing the extent of anode pull out during disassembly.

area is represented in Fig. 10B. Notice that in some areas the polymeric material appears to be embedded in the aggregate of particles. Fig. 10C was included to show that the microstructure of the separator still appears to be intact, suggesting that the binder might be the polymeric material seen in A and B. Fig. 10D shows another region on the anode surface that has embedded particles with the highest concentration of Ni detected so far. Further investigation will be required to unambiguously determine the source of this material.

5. Conclusion

Cells based on NMC/graphite, containing PVDF binders in the positive and negative electrodes, were systematically overcharged to 100%, 120%, 140%, 160%, 180%, and 250% SOC. At 250% SOC the cell vented.

Inhomogeneities across the laminate surface were evident during disassembly. Surface discoloration along with delamination of the active layer from the collector increased with an increasing state of charge. In addition, the collector had a dull and a shiny side with significantly more delamination of the active material from the shiny side, particularly at 180% and 250% SOC.

SEM/EDS of the anodes revealed several state-of-overcharge-dependent trends. Starting at 120% SOC, dendrites were first observed and increased in concentration as the SOC increased; an indication of the increasing reactions of Li with electrolyte components. As the overcharge increased, the morphology of Li deposits changed, with thicker coating on dendrite structures and the formation of more lobular structures (presumably Li deposits). Transition metals were associated with nanoparticles embedded in the coating of Li deposits, and increased in concentration with increasing overcharge.

As the overcharge increased, particularly at 180% SOC, the evolution of an increasingly complex morphology was evident in the formation of multilayer structures over the graphite particles. At 250% SOC, previously unobserved polymeric strands were seen on the anode surface, a possible indication of the beginning of binder breakdown.

Acknowledgments

The work at Argonne National Laboratory was supported by the U.S. Department of Energy (DOE), Office of Energy Efficiency and Renewable Energy (EERE), Vehicle Technologies Office (VTO). Argonne National Laboratory is operated for DOE Office of Science by UChicago Argonne, LLC, under contract number DE-AC02-06CH11357.

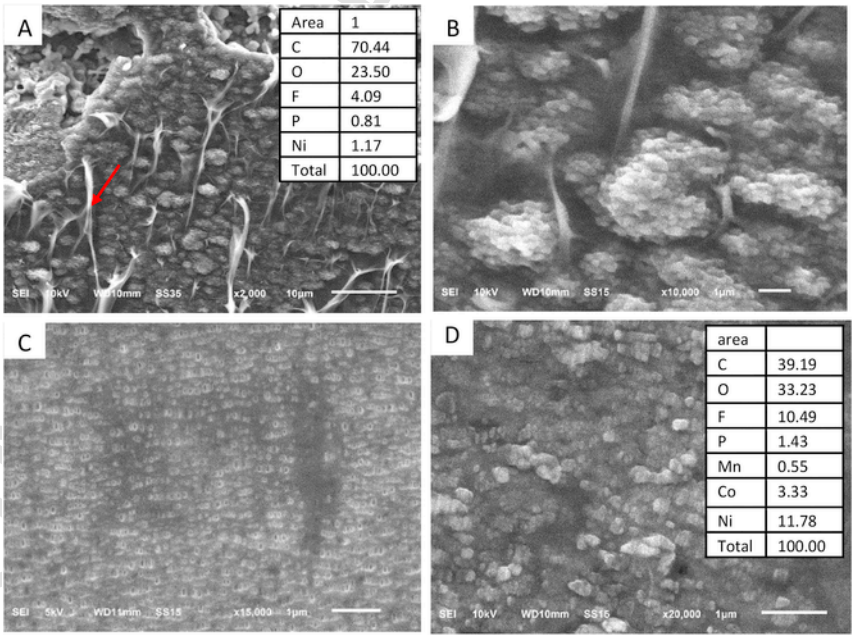

Fig. 10. Surface of 250% SOC anode showing A) polymeric strands on anode, B) polymeric material in between surface aggregates, C) exposed separator, and D) another area of anode surface associated with the highest concentration of Ni detected.

The work at Oak Ridge National Laboratory, managed by UT Battelle, LLC, for the U.S. Department of Energy (DOE) under contract DE-AC05-00OR22725, was sponsored by the Office of Energy Efficiency and Renewable Energy (EERE), Vehicle Technologies Office, Applied Battery Research.

Sandia National Laboratories is a multi-mission laboratory managed and operated by National Technology and Engineering Solutions of Sandia, LLC., a wholly owned subsidiary of Honeywell International, Inc., for the U.S. Department of Energy's National Nuclear Security Administration (NNSA) under contract DE-NA0003525.

Appendix A. Supplementary data

Supplementary data related to this article can be found at https://doi.org/10.1016/j.jpowsour.2018.01.009.

References

[1] H.-J. Noh, S. Youn, C.S. Yoon, Y.-K. Sun, J. Power Sources 233 (2013) 121–130.
[2] M. Ouyang, D. Ren, L. Lu, J. Li, X. Feng, X. Han, G. Liu, J. Power Sources 279 (2015) 626–635.
[3] J. Wen, Y. Yu, C. Chen, Mater. Express 2 (3) (2012).
[4] A.J.-W. Wen, D.-W. Zhang, C.-H. Chen, C.-X. Ding, Y. Yu, J. Maier, J. Power Sources 264 (2014) 155–160.
[5] B.J. Lamb, C.J. Orendorff, K. Amine, G. Krumdick, Z. Zhang, L. Zhang, A.S. Gozdz, J. Power Sources 247 (2014) 1011–1017.
[6] C.K.A. Narayana, M.D. Casselman, C.F. Elliot, S. Ergun, S.R. Parkin, C. Risko, S. Odom, ChemPhysChem 16 (2015) 1179–1189.
[7] Q.F. Yuan, F. Zhao, W. Wang, Y. Zhao, Z. Liang, D. Yan, Electrochim. Acta 178 (2015) 682–688.
[8] Y. Makimura, T. Sasaki, H. Oka, C. Okuda, T. Nonaka, Y.F. Nishimura, S. Kawauchi, Y. Takeuchi, J. Electrochem. Soc. 163 (2016) A1450–A1456.
[9] W. Cui, Y.-B. He, Z.-Y. Tang, Q.-H. Yang, Q. Xu, F.-Y. Su, L. Ma, J. Solid State Electrochem. 16 (2012) 265–271.
[10] A.W. Golubkov, S. Scheikl, R. Planteu, G. Voitic, H. Wiltsche, C. Stangl, G. Fauler, A. Thaler, V. Hacker, RSC Adv. 5 (2015) 57171–57186.
[11] R.A. Leising, M.J. Palazzo, E.S. Takeuchi, K.J. Takeuchi, J. Electrochem. Soc. 148 (2001) A838–A844.
[12] F. Xu, H. He, Y.D. Liu, C. Dun, Y. Ren, Q. Liu, M.-X. Wang, J. Xie, J. Electrochem. Soc. 159 (2012) A678–A687.
[13] F. Larsson, B.-E. Mellander, J. Electrochem. Soc. 161 (2014) A1611–A1617.
[14] Y. Liu, J. Xie, J. Electrochem. Soc. 162 (2015) A2208–A2217.
[15] W. Lu, C.M. López, N. Liu, J.T. Vaughey, A. Jansen, D.W. Dees, J. Electrochem. Soc. 159 (2014) A566–A570.
[16] J. Arai, Y. Okada, T. Sugiyama, M. Izuka, K. Gotoh, K. Takeda, J. Electrochem. Soc. 162 (2015) A952–A958.
[17] A. Devie, M. Dubarry, B.Y. Liaw, J. Electrochem. Soc. 162 (2015) A1033–A1040.
[18] I. Bloom, et al., (2017).
[19] J. Bareno, et al., (2017).
[20] J. Li, C. Daniel, S.J. An, D.L. Wood III, MRS Adv. 1 (15) (2016) 1029–1035.
[21] J.Y. Howe, L.A. Boatner, J.A. Kolopus, L.R. Walker, C. Liang, N.J. Dudney, C.R. Schaich, J. Mater. Sci. 47 (3) (2012) 1572–1577.
[22] F. Orsini, A. Du Pasquier, B. Beaudoin, J.M. Tarascon, M. Trentin, N. Langenhuizen, E. De Beer, P. Notten, J. Power Sources 76 (1998) 19–29.
[23] J.-G. Zhang, W. Xu, W.A. Henderson, Lithium metal anodes and rechargeable lithium metal batteries, Chapter 2 Springer Mater. Sci. 249 (2017).
[24] J. Steiger, D. Kramer, R. Monig, J. Power Sources 261 (2014) 112–119.
[25] R. Bouchet, Nat. Nanotechnol. 9 (August 2014) 572–573.
[26] D. Below, M.-H. Yang, J. Solid State Electrochem. 12 (2008) 885–894.
[27] H.J. Bang, H. Joachin, H. Yang, K. Amine, J. Prakash, J. Electrochem. Soc. 153 (4) (2006) A731–A737.
[28] Q.-F. Yuan, F. Zhao, W. Wang, Y. Zhao, Z. Liang, D. Yan, Electrochim. Acta 178 (2015) 682–688.
[29] D. Aurbach, E. Zinigrad, Y. Cohen, H. Teller, Solid State Ionics 148 (2002) 405–416.
[30] D. Aurback, J. Power Sources 89 (2000) 206–218.
[31] D. Zane, A. Antonini, M. Pasquali, J. Power Sources 97–98 (2001) 146–150.
[32] S.J. An, J. Li, C. Daniel, D. Mohanty, S. Nagpure, D.L. Wood III, Carbon 105 (2016) 52–76.
[33] D. Lu, Y. Shao, T. Lozano, W.D. Bennett, G.L. Graff, B. Polzin, J. Zhang, M.H. Engelhard, N.T. Saenz, W.A. Henderson, P. Bhattacharya, J. Liu, J. Xiao, Adv. Energy Mater. 5 (2015) 1400993.
[34] R. Spotnitz, J. Franklin, J. Power Sources 113 (2003) 81–100.
[35] P. Verma, P. Maire, P. Novak, Electrochim. Acta 55 (2010) 6332–6341.